Computers and Electronics in Agriculture 222 (2024) 109092

Contents lists available at ScienceDirect

Computers and Electronics in Agriculture

journal homepage: www.elsevier.com/locate/compag

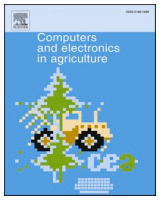

Original papers

Assessing mixed-pixels effects in vineyard mapping from Satellite: A proposal for an operational solution

De Petris S.*, Sarvia F., Parizia F., Ghilardi F., Farbo A., Borgogno-Mondino E.

Department of Agriculture, Forestry and Food Sciences, University of Torino (Italy), L.go Braccini 2, Grugliasco (TO) 10095, Italy

ARTICLE INFO

Keywords:
NDVI
Vineyards
Spectral Unmixing
Sentinel-2
UAV

ABSTRACT

Satellite-based multispectral remote sensing in the wine sector is expanding, aiming at improving vineyard management for both environmental sustainability and vine quality/yield. However, vineyards present a discontinuous vegetative surface, with rows of vines alternating with background areas (bare soil or other vegetation). This irregular pattern adversely affects multispectral satellite data from public and research missions (such as Sentinel 2 and Landsat 8/9, etc.), which operate at lower geometric resolutions. When inter-row spaces become overgrown with other vegetation that occasionally requires mowing, the average spectral response of the pixels changes significantly. Consequently, spectral information specific to the vines is obscured by a complex signal, potentially leading to incorrect conclusions if directly analyzed. To address this issue, this study introduces a novel method for recovering the spectral signal of vines, specifically focusing on NDVI from Sentinel-2 data (S2).The approach relies on the estimation of the local NDVI value of vines by a least squares techniques based on the application of a spectral unmixing technique operated in the space domain using a moving window surrounding the pixel for which the estimation is required for. At each moving window step, NDVI values of only grapevines (at satellite resolution i.e., 10 m per 10 m) were estimated and mapped using as main inputs the S2 NDVI values and the grapevine fraction cover values retrieved by high resolution UAV imagery. Results shows a 16 % relative error in NDVI measurements for vines.

1. Introduction

Satellite-based multispectral remote sensing is heavily entering the viticultural context aiming at supporting improvement of vineyard management in terms of environmental sustainability and vines quality/yield (Priori et al., 2013). In this framework, satellite-based optical remote sensing has already proved to be an effective technique for mapping vines vigor in both the space and time domains (Giovos et al., 2021; Hall et al., 2002; Johnson et al., 2003). Maps of spectral indices are known to be useful to support viticultural practices, thus improving wine quality and mitigating environmental impacts. Nevertheless, vineyards represent a challenge for satellite imagery from open and scientific missions (e.g. Sentinel 2, Landsat 8/9, etc.) because grapevine canopies alternate with inter-rows background making the recorded signal a mixed one (Hall et al., 2008).

Consequently, spectral-related information about vines is hidden in a complex signal that, if directly interpreted, could lead to wrong deductions (Ferreiro-Arman et al., 2006). Vineyard landscape is ordinarily characterized by a regular pattern of rows (i.e., grapevines) interleaved by inter-rows sizing always more than 1.5 m. This guarantee sunlight penetration needed for the development of both canopy and grapes (Reynolds et al., 1996; Winkler, 1969). Spontaneous vegetation systematically grows within inter-row areas. A difficult situation occurs when inter-rows are covered by other vegetation (e.g. grass) that, time to time, has to be mowed, thus significantly changing the average spectral response of pixels along the year. It is worth to remind that grass maintenance in vineyards is one of the most important rules of the European soil conservation policy as reported in the Standards of Good Agricultural and Environmental Condition (GAEC) created by Council Regulation No. 73/2009 (Bagagiolo et al., 2018). This regulation determines that, continuously, more and more vineyards move to this type of situation. In Northern Italy, in particular, mechanization and other inter-rows management practices, like tillage and bare soil preservation, are going to be abandoned (Biddoccu et al., 2013). Unfortunately, this "green" trend introduce a further problem when interpreting vineyards behavior from satellite multi-spectral data, by substituting the "static" spectral contribution from soil with the more "dynamic" one from other vegetation. This adds confusion in the spectral interpretation of

* Corresponding author.
E-mail address: samuele.depetris@unito.it (S. De Petris).

https://doi.org/10.1016/j.compag.2024.109092
Received 6 December 2023; Received in revised form 21 May 2024; Accepted 22 May 2024
Available online 30 May 2024

differences possibly related to vines, since grass-related variations cannot be distinguished from the vines-related ones. This difficulty concerns both differences among vineyards zones as recordable at the same date, and differences at the same location along time. Moreover, one has also to consider that, from one side vegetated inter-rows express their own phenology, from the other one they have to be managed by mowing (to minimize the competition with vines) and, for sure, they are occasionally compacted by operative machineries (Biddoccu et al., 2014).

To address this problem, one possible solution relies on the adoption of high-resolution satellite,e.g., WorldView-2 (Karakizi et al., 2016), or UAV (Uncrewed Aerial Vehicle) imagery (Pádua et al., 2022). Some satellite missions can acquire data with a very high geometric resolution (i.e., about half a meter), but these data are often offered by private companies with a significant cost for users. Moreover, they generally require high data processing skills and regularity of acquisition is not guaranteed (Helman et al., 2018; Rahman et al., 2018; Van Beek et al., 2013). Similarly, UAV acquisitions can provide images at a very high resolution (about 1–2 cm), but they call the users to a further higher level of technical skills (included the photogrammetry-related ones) and the associated costs are significant, as well (Borgogno Mondino, 2018; Borgogno Mondino and Gajetti, 2017). Moreover, although possible, mapping solutions based on high-resolution satellite images/UAV cannot be considered if past acquisitions are needed for multi-temporal analysis.

With these premises, satellites missions providing continued, free and scientifically processed data at a medium spatial resolution, presently, appear to be the most affordable solution for a trustable technology transfer. In particular, the Sentinel-2 mission (S2) by the European Copernicus program, can be efficiently used in agriculture thanks to its high spectral, geometric and temporal resolution (Giovos et al., 2021). S2 data are, in fact, known to be useful for: crop phenology monitoring (Misra et al., 2020), land use/cover mapping (Kaul and Sopan, 2012; Phiri et al., 2020), urban greenness mapping (Borgogno-Mondino and Fissore, 2022; De Petris et al., 2021); precision farming (Farbo et al., 2022; Segarra et al., 2020), ecosystems characterization (Pastick et al., 2020; Sarvia et al., 2022a), crop yield estimation (Marshall et al., 2022; Soriano-González et al., 2022), supporting insurance policies in crop damage estimation (Borgogno-Mondino et al., 2019; F et al., 2020; Greatrex et al., n.d) and Common Agricultural Policy controls (Filippo et al., 2022; Sarvia et al., 2022b). In spite of these great amount of works involving S2 data, only in few of them the spectral unmixing problem is considered (Clasen et al., 2015). A rare example comes from Borgogno-Mondino et al. (2022) concerning the proposal of a spectral-unmixing procedure for recovering the "pure" spectral response of pomegranates in Southern Italy and relating them to the midday stem water potential. In this work, authors proved that, if a theoretical fixed pattern defining rows/inter-rows spacing is considered results are unsatisfactory (Borgogno-Mondino et al., 2022).

To separate the spectral mixture between vines and inter-rows from satellite recorded signal, in this work, with a special focus on NDVI from Sentinel-2 data, a possible solution for only-vines spectral signal recovering is proposed, based on a-priori accurate mapping of vineyard pattern by Uncrewed Aerial Vehicle (UAV). To ensure robustness of deductions, the same procedure was applied on 9 different vineyards spread across Piemonte Region (NW Italy). The approach relies on the estimation of the local NDVI value of vines by a least squares techniques based on the application of a spectral unmixing technique operated in the space domain using a moving window surrounding the pixel for which the estimation is required for. At each moving window step, NDVI values of only grapevines (at satellite resolution i.e., 10 m per 10 m) were estimated and mapped using as main inputs the S2 NDVI values and the grapevine fraction cover values retrieved by high resolution UAV imagery. Accuracy and sensitivity of the method were assessed by comparing the unmixed NDVI maps derived from S2 data with the correspondent ones from the available multispectral acquisitions by UAV.

2. Materials and methods

2.1. Study sites

The area of interest (AOI) is located in the Piemonte region (NW-Italy) and develops across 3 provinces, namely Alessandria, Asti and Cuneo, and 7 municipalities (Mango, Castiglione Tinella, Loazzolo, Castel Rocchero, Sessame, Trezzo Tinella, Alice Bel Colle). Within AOI, 9 sites, corresponding to 9 vineyards, were selected (Fig. 1a) as representatives of the typical landscape of Langhe-Roero and Monferrato that is included in the UNESCO World Heritage List (Assumma et al., 2016). Vineyards boundaries were obtained as a polygon vector layer from the Piemonte Region farming registry. These were provided with a nominal scale of 1:2000, updated 2022 ("Anagrafe agricola del Piemonte – Sistema Piemonte – Regione Piemonte. Available online: https://servizi.regione.piemonte.it/catalogo/anagrafe-agricola-piemonte (Accessed on 25/05/2023)," n.d.) and georeferenced in the WGS84 UTM 32 N coordinate system. Sample vineyards correspond to different vine types that are cultivated in diverse environmental and agronomic conditions, i.e. Moscato Bianco, Dolcetto, Chardonnay, Pinot Nero and Nebbiolo (Fig. 1b).

2.2. Remotely sensed data

2.2.1. Reference data

Nowadays aerial images acquired by anUAV are adopted to accurately survey 3D and spectral features of vineyards. In particular, a DJI Phantom 4 (DJI P4) Multispectral quadcopter (DJI, 2023) was used. DJI P4 is equipped with an RGB CMOS camera and a multispectral sensor recording the following spectral ranges: blue band (450 nm ± 16 nm), green band (560 nm ± 16 nm), red band (650 nm ± 16 nm), red edge band (730 nm ± 16 nm), near infrared (NIR) band (840 nm ± 26 nm). An incoming Sunlight Irradiance sensor (ILS) is coupled with the sensor enabling a rough spectral calibration of images needed for reflectance recovery from raw data. These bands can be efficiently used to compute different spectral indices (DJI, 2023; Narmilan et al., 2022; Sakamoto et al., 2022; Wang et al., 2022). In addition, the DJI P4 is supplied, equipped with two GNSS (global navigation satellite system) receivers: one on board of the UAV (rover), the other located at the ground on a fix position (master). The system makes possible to position the UAV in RTK (Real Time Kinematic), solving instantaneously the relative baseline master-rover and linking the master station to a correction network operating in Virtual Reference Station mode (VRS). During all the 9 surveys operated for this work, the GNSS master station position was solved using the Interregional Piemonte-Lombardia SPIN-GNSS service (https://www.spingnss.it/spiderweb/frmIndex.aspx). This made possible to position images (focal point) with a 3D precision of about 0.037 m. Approximated attitude angles recorded by the on-board inertial measurement unit (IMU) were used during the image block bundle adjustment step. Flights were operated on the 23rd and 24th August 2023, from an altitude AGL (above ground level) of 80 m. Forward and side overlap were set to 80 % and 70 %, respectively. The average GSD (ground sampling distance) resulted to be about 5 cm. To minimize shadow effects, surveys were performed between 11 AM and 2 PM local time (GMT + 2 in summertime). In this period of the year, in this area, grapevine is in its ripening phenological phase (BBCH scale = 85). This ensured that vines canopy and fruits area were already developed, and row/inter-row covers could be assumed no more significantly changing.

2.2.2. Satellite data

Copernicus Sentinel-2 (S2) data detected by onboard multispectral instrument were used for this work. It is worth noting that these data are provided free of charge, featuring a GSD of 10 m for both the Near-Infrared (NIR) and Red spectral bands. Additionally, the temporal resolution of S2 data, at 5 days, is particularly well-suited for vineyard monitoring (Table 1). A single S2 Level-2A scene –T32TMQ- (calibrated

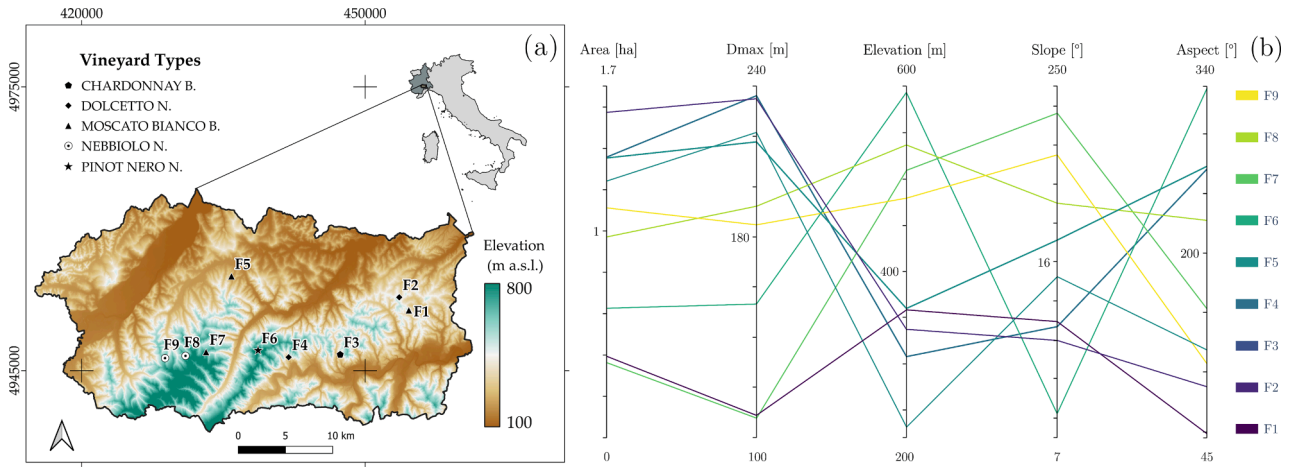

Fig. 1. (a) Digital Terrain Model of AOI (SRTM 90 m) and sample vineyards location per vineyard types. Reference coordinates system is WGS84/UTM 32 N. (b) parallel coordinates chart showing the behavior of sample vineyards and morphological factors.

at the bottom of the atmosphere) was acquired on 24th August 2023 with cloud coverage less than 5 %. This data was obtained from the Copernicus SciHub geoportal (www.). The date of acquisition ensures proper comparability with UAV data.

2.3. Data pre-processing

Nine blocks were acquired by DJI P4, each averagely made of about 300 images. All image blocks were photogrammetrically processed in the Pix4D Mapper software (Pix4D S.A, 1008 Prilly, Switzerland) which allows for accurate geometric and radiometric calibration. Image block bundle adjustment was carried according to an "adjusted" direct georeferencing approaching based on GNSS and IMU measurements as starting estimates of Exterior Orientation Parameters (Forlani et al., 2018; Nesbit et al., 2022; Teppati Losè et al., 2020; Westoby et al., 2012). Internal camera orientation parameters were also re-estimated during the adjustment. Final image orientation resulted to have a theoretical (after the adjustment) horizontal and vertical mean error of about 0.009 m and 0.030 m, respectively. Nine dense 3D point clouds were generated from the blocks, with an average point density of about 150p/m^2. Point clouds were automatically classified by Pix4D software to separate ground from not-ground points and the correspondent Digital Surface Models (DSM) and Digital Terrain Models (DTM) generated by regularization, setting a geometric resolution of 0.1 m. A canopy height model (CHM) of the vineyard was obtained for all the blocks by differencing DSM and DTM. The DSM was used to generate the correspondent multispectral orthomosaic (GSD = 0.1 m) for all the investigated vineyards. A spectral calibration step was achieved in Pix4D to recover approximated reflectance values from the raw data using the measurements from the available solar irradiance sensor (also called irradiance light sensor – ILS) plugged on the top of the UAV (PIX4D Support, 2023). This sensor allows to measure the sun irradiance for each spectral band. Finally, in PIX4D software reflectance values were recovered by the ratio between calibrated radiance values recorded by multispectral sensor and sun irradiance values recorded by ILS sensor. The calibrated red and NIR bands of the orthomosaics were finally combined to compute the Normalized Difference Vegetation Index (NDVI) map of sample vineyards (GSD = 0.1 m). These high resolution NDVI maps – hereafter called $NDVI^{UAV}(x,y)$ – were assumed as reference data to validate the proposed approach, being able to map separately the expected NDVI value for vines and for inter-rows.

Starting from the red and NIR S2 L2A bands, the correspondent NDVI map – hereafter called $NDVI^{S2}(x,y)$- was computed with a geometric resolution of 10 m. This layer was adopted as basic input for the proposed method (see following sections).

Table 1
S2 band technical features: central wavelength, bandwidth, GSD, radiometric resolution and temporal resolution.

Spectral Band	Central Wavelength (nm)	Band Width (nm)	GSD (m)
B1 (Aerosol)	443	20	60
B2 (Blue)	490	65	10
B3 (Green)	560	35	10
B4 (Red)	665	30	10
B5 (Red Edge 5)	705	15	20
B6 (Red Edge 6)	740	15	20
B7 (Red Edge 7)	783	20	20
B8 (Near Infrared)	842	115	10
B8A (Near-Infrared Plateau)	885	20	20
B9 (Water Vapor)	945	20	60
B10 (Cirrus)	1380	30	60
B11 (Short-Wave Infrared 1)	1610	90	20
B12 (Short-Wave Infrared 2)	2019	180	20
Radiometric resolution	12 bits		
Nominal Temporal resolution	5 days		

2.4. Data processing

The workflow of this work is reported in Fig. 2 and aims at giving an estimate of the NDVI value of the solely grapevine plants starting from a mixed signal (vines + background) that ordinarily characterizes S2 pixels. This is achieved by integrating the detailed geometric content from UAV acquisitions, useful for accurately mapping the vineyard pattern, with the spectral content (NDVI) from S2 images. UAV multispectral data were also used to validate the method, assuming NDVI values of vines from UAV data as the reference ones.

2.4.1. Row / inter-row mapping

The above mentioned CHMs and the correspondent NDVI calibrated map from UAV, were used to map vineyards pattern in terms of row and inter-row, with a native resolution of 0.1 m. This was achieved by testing the joint satisfaction of the following 2 conditions to recognize rows (vines): CHM > 0.5 m and NDVI > 0.3 (Burgan, 1993; Ormsby et al., 1987; Zhang et al., 2003). The first condition takes care about the geometry of rows where vegetated fraction is expected to develop about 0.5 m above ground level. The second condition looks for only vegetated (from poorly to high) pixels along the row, thus limiting eventual artifacts always present in CHM.

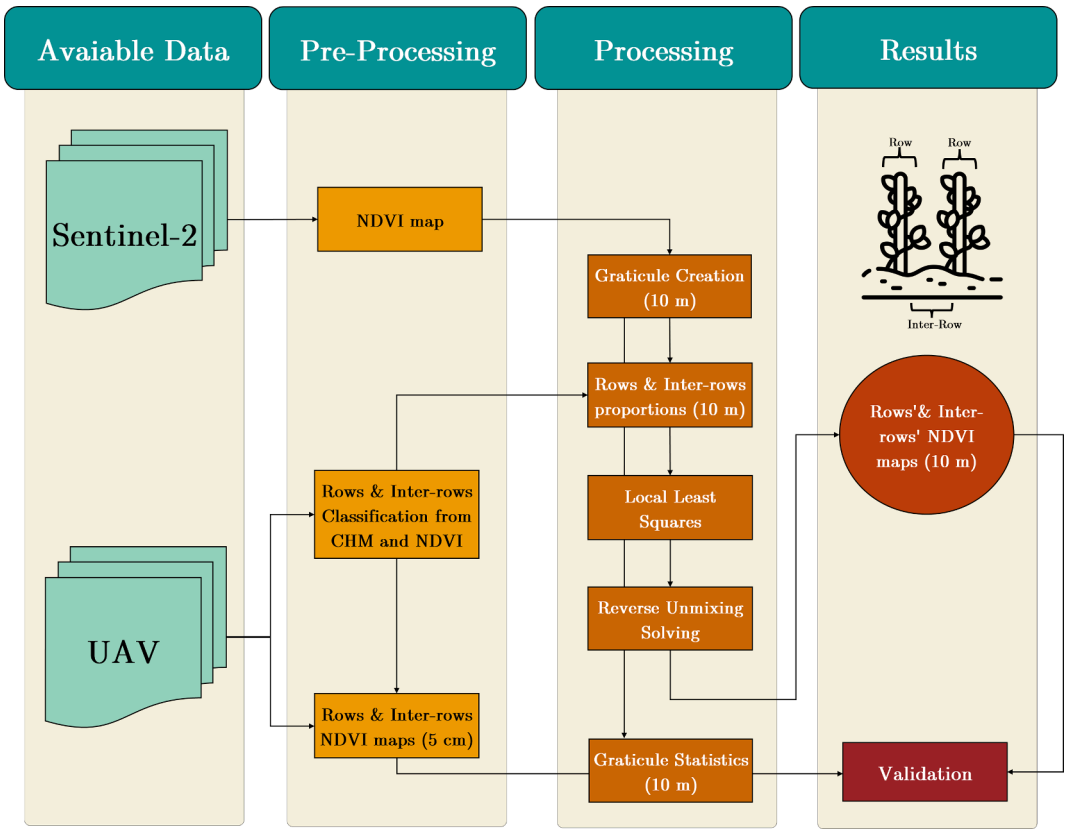

Fig. 2. Adopted workflow based on the integration of Sentinel-2 L2A and multispectral UAV images. Both the data were pre-processed to generate adequate NDVI maps. A spatially based local least squares estimation was used to un-mix S2 data and obtaining reliable estimates of "pure" NDVI for both vines and inter-row cover.

This strategy made possible to separate vineyards areas with vines, from the ones hosting other type of surfaces (bare soil or grass), generating an accurate map of vineyard layout (hereafter called *G-IR* classification), able to address the next un-mixing operations. *G-IR* binary classification has the same geometric resolution of the $NDVI^{UAV}(x,y)$, i.e. 0.1 m. Two new raster layers mapping, separately, the NDVI of grapevines – $NDVI_G^{UAV}(x,y)$- and background –$NDVI_{IR}^{UAV}(x,y)$ – were finally generated with reference to *G-IR*.

Finally, to ensure a proper comparison with S2-derived NDVI values, a vector graticule layer (*G*) was created with a cell size of 10 m aligned to $NDVI^{S2}(x,y)$. The grapevine fraction cover (area percentage) was assigned to each *G* cell by zonal statistics from *G-IR* and *G* rasterized correspondently to finally generate the raster layer $f_G(x,y)$, mapping the expected vines fraction cover within each S2 pixel.

2.4.2. Spectral linear mixture model

Vineyards are characterized by a regular pattern of grapevine rows and inter-rows. S2 imagery provides a too coarse resolution if compared with the size of the vineyard pattern traits. Consequently, recorded reflectance is always something mixed as resulting from the joint contribution of vines and inter-rows fraction within the ground footprint of each S2 pixel. When longing for adoption of S2 data to describe vines behavior, it is mandatory a pre-processing step aimed at recovering the spectral contribution of the solely-vine fraction from the native mixed pixel. Although the mixing process could be not-linear, linear models are widely used (Hu et al., 1999). In this work, a spectral linear model was adopted, assuming that the local spectral signal only depends on 2 endmembers that participate proportionally to their fraction cover (known) in the considered pixel. The first endmember is grapevine canopy (G); the second is inter-row cover (IR). The latter can, in general, results from a mixture of bare soil and grass; specifically in AOI inter-row tillage is rarely applied (Bagagiolo et al., 2018). One can, therefore, assume that inter-row zones are mainly dominated by other vegetation along its entire phenological active period.

With these premises, the proposed spectral linear mixture model (LMM) was applied according to eq. (1).

$$NDVI^{S2}(x,y) = f_G(x,y) \bullet NDVI_G + \left[1 - f_G(x,y)\right] \bullet NDVI_{IR} \quad (1)$$

where $NDVI^{S2}(x,y)$ is the S2-derived NDVI at the generic position, $f_G(x,y)$ is the fraction cover at that position, $NDVI_G$ and $NDVI_{IR}$ are the two unknown NDVI values of grapevine and inter-row, respectively.

To test LMM assumption, linear regression involving all vineyards pixels was fitted between S2-retrieved NDVI values and the correspondent ones computed applying eq.1 involving $f_G(x,y)$ and the correspondent means of $NDVI_{G,IR}^{UAV}(x,y)$ computed using G.

2.4.3. Recovering NDVI of vines through local least squares and reverse unmixing

To map separately the estimates of $\widehat{NDVI}_G$ and $\widehat{NDVI}_{IR}$ starting from the native ones from S2 imagery, an approach based on a spatial approach to least squares estimation was developed. It somehow reverses the ordinary spectral un-mixing paradigm and moves from the space of the bands into the physical space, assuming that a spatial autocorrelation exists among within vineyards NDVI values at the S2 scale. In fact, starting from the a-priori known (from UAV) fraction covers of the 2 involved endmembers, corresponding to an appropriate number (k) of neighbours surrounding the position the estimate is required for, the system of eq. (2) is locally solved using a moving window approach. The underlying (and forcing) hypothesis is that the local solution for the "pure" NDVI estimates of endmembers at the investigated position is somehow consistent (equal) to the one of its neighbour pixels.

$$\begin{cases} NDVI_{S2}^{1} = f_G^1 \bullet NDVI_G + \left[1 - f_G^1\right] \bullet NDVI_{IR} \\ NDVI_{S2}^{2} = f_G^2 \bullet NDVI_G + \left[1 - f_G^2\right] \bullet NDVI_{IR} \\ \vdots \\ NDVI_{S2}^{k} = f_G^k \bullet NDVI_G + \left[1 - f_G^k\right] \bullet NDVI_{IR} \end{cases} \quad (2)$$

where $NDVI_{S2}^{k}$ and f_G^k are the S2 NDVI values and grapevine fraction cover at the *k-th* pixel within the moving window; $NDVI_G$ and $NDVI_{IR}$ are the unknown NDVI local values, specific for vines and background (endmembers), assumed as equal in the involved portion of vineyard.

The expected Least Squares solution ($\widehat{\vartheta}$), i.e. the unmixed estimates of the local $NDVI_G$ and $NDVI_{IR}$ (namely,$\widehat{NDVI}_G$ and $\widehat{NDVI}_{IR}$), is given by eq. (3)

$$\widehat{\vartheta} = \left(A^T A\right)^{-1} A^T L = \begin{bmatrix} \widehat{NDVI}_G \\ \widehat{NDVI}_{IR} \end{bmatrix} \quad (3)$$

where $A = \begin{bmatrix} f_G^1 & 1 - f_G^1 \\ f_G^2 & 1 - f_G^2 \\ \cdots & \cdots \\ f_G^k & 1 - f_G^k \end{bmatrix}$; $L = \begin{bmatrix} NDVI_{S2}^{1} \\ NDVI_{S2}^{2} \\ \cdots \\ NDVI_{S2}^{k} \end{bmatrix}$; ^{T} is the transpose matrix.

Unfortunately, given the obvious correlation between vines and background fraction covers, a strong multicollinearity is expected for $\boldsymbol{A}$, thus compromising the solution. To take care about this problem, the Tikhonov's regularization (Hoerl et al., 1975; Qian, 2017; Tikhonov, 1963) was used and eq.3 was moved to eq.4.

$$\widehat{\vartheta} = \left(A^T A + \lambda I\right)^{-1} A^T L \quad (4)$$

where, $\boldsymbol{I}$ is the identity matrix and λ is Tikhonov parameter.

Once the system was built and solved at whatever position within the vineyard the $\widehat{NDVI}_G$ and $\widehat{NDVI}_{IR}$ maps were finally generated (hereafter called $\widehat{NDVI}_G(x,y)$ and $\widehat{NDVI}_{IR}(x,y)$ respectively) with a GSD = 10 m.

The separability between $\widehat{NDVI}_G$ and $\widehat{NDVI}_{IR}$ distributions was tested by the Kolmogorov-Smirnov test (KS) for each sample vineyard.

Moreover, the theoretical uncertainty of $\widehat{NDVI}_G$, $\sigma_G(x,y)$, and $\widehat{NDVI}_{IR}$, $\sigma_{IR}(x,y)$, were also estimated and mapped using eq. (5).

$$\sigma_{G,IR} = \sqrt{[\Sigma_\vartheta]_{ii}}, \Sigma_\vartheta = \frac{v^T v}{m-n}\left(A^T A + \lambda I\right)^{-1} A^T L \quad (5)$$

where $[\Sigma_\vartheta]_{ii}$ is the *i-th* diagonal element of the covariance matrix (Σ_ϑ) of $\widehat{\vartheta}$; v is the vector of residuals; m and n are respectively the number of neighbours and unknowns (endmembers), respectively.

2.5. Validation

To validate $\widehat{NDVI}_G$ and $\widehat{NDVI}_{IR}$ estimates they were compared with the ones from UAV ($NDVI^{UAV}$). For this task, G-IR was initially used to isolate grapevine and inter-row pixels in $NDVI^{UAV}$. Two new raster layers ($NDVI_G^{UAV}$ and $NDVI_{IR}^{UAV}$) were obtained. Mean (μ_G and μ_{IR}) and standard deviation (s_G, s_{IR}) values from $NDVI_G^{UAV}$ and $NDVI_{IR}^{UAV}$, respectively, were finally computed through ordinary zonal statistics, for all the G cells. Estimate errors were mapped according to eq. (6).

$$\varepsilon_{G,IR}(x,y) = \left|\widehat{NDVI}_{G,IR}(x,y) - \mu_{G,IR}(x,y)\right| \quad (6)$$

To investigate error type, the bias-variance decomposition (Bouckaert, 2008; Domingos, 2000) was applied at pixel level (eq. (7).

$$\left[\varepsilon_{G,IR}(x,y)\right]^2 = Tr(\Sigma_\vartheta) + Bias^2 \quad (7)$$

where *Tr* is the trace of the local Σ_ϑ and *Bias* the bias term. at each position is known, bias term can be computed and its weight on $\left[\varepsilon_{G,IR}(x,y)\right]^2$ evaluated simply by ratio. This analysis allows to detect the weights of biases or the parameters variance in proposed methods. Finally, the mean absolute percentage error (MAPE) was also computed at vineyard level to give a more effective quantification of estimate error.

2.6. Sensitivity analysis

The proposed un-mixing method requires that 2 operational parameters are set: the regularization coefficient (λ) and the moving window size (W). A first sensitivity analysis was therefore performed looking for an optimal solution. This was achieved through a *R* v.4.1 (R Development Core Team, 2013) self-developed procedure in charge of iteratively changing the value of λ (in the range 0.01–0.1) and W. The latter was changed starting from 3 x 3 pixels up to the value corresponding to the smaller size of the investigated vineyard. For all combinations the correspondent MAPE was computed and represented as a 3D surface (λ, *W, MAPE*) looking for its minimum.

Another sensitivity analysis was performed to assess the theoretical effect of the precision of fraction cover estimates ($f_G(x,y)$) on $\widehat{NDVI}_G$. In particular, this analysis was performed in order to highlight operative limits of proposed approach. In fact, $f_G(x,y)$ is not a direct measure but it resulted from a mapping procedure aiming at classifying vines canopy. Several methods can be used to this task affected by different fraction cover precisions. In this work, we used high resolution UAV images to retrieve such an information. Nevertheless, one can wonder about the effect of relative error in the $f_G(x,y)$ onto $\widehat{NDVI}_G$. To explore this dependence, the condition number (Baboulin et al., 2009; Jia and Li, 2013) was adopted. Condition number (K_2) relates the upper-bound of the relative error of the estimates (i.e. $\widehat{NDVI}_G$) with the expected relative error of coefficients (elements of A matrix, i.e., fractions cover) see eq.8.

$$\frac{\|\delta\widehat{NDVI}_G\|}{\|\widehat{NDVI}_G\|} \leq K_2 \frac{\|\delta A\|}{\|A\|} \quad (8)$$

where $\| \bullet \|$ is the Euclidean norm, $\delta\widehat{NDVI}_G$ is the absolute error of the endmember NDVI values for grapevine canopy; δA are the perturbed design matrix. This made possible to compute K_2 for each step of W and mapped across the vineyard.

3. Results

3.1. Row /Inter-row mapping

An example of $f_G(x,y)$ as mapped from G-IR is reported in Fig. 3.

According to Fig. 3a it can be noticed that the vines-related fraction cover is always smaller than the inter-row one. Specifically, for F3, Fig. 3b shows that it ranges between 6 % and 25 % with a mean value of 18 %. These values appear to be fairly stable for all the investigated vineyards (Fig. 3c). Two exceptions come from F4 and F6 where the median value of the vines fraction cover values resulted to be 45 % and 38 %, respectively. Differently, vineyard showed significant differences in terms of internal variability. For example, Fig. 3c shows a small variability for F7 around a median value of fraction cover of about 18 %. Conversely, F4 shows a highly different median value associated to a great variability where the fraction cover of vines ranges between 20 % and 70 %. These differences can be probably related to different vine types or canopy management in vineyards. Similar mean values of f_G were, in fact, found within Moscato and Nebbiolo corresponding to F1, F5, F7 and F8, F9 respectively.

3.2. Spectral linear mixture model

Fig. 4 shows the correlation between S2-derived NDVI, and the ones

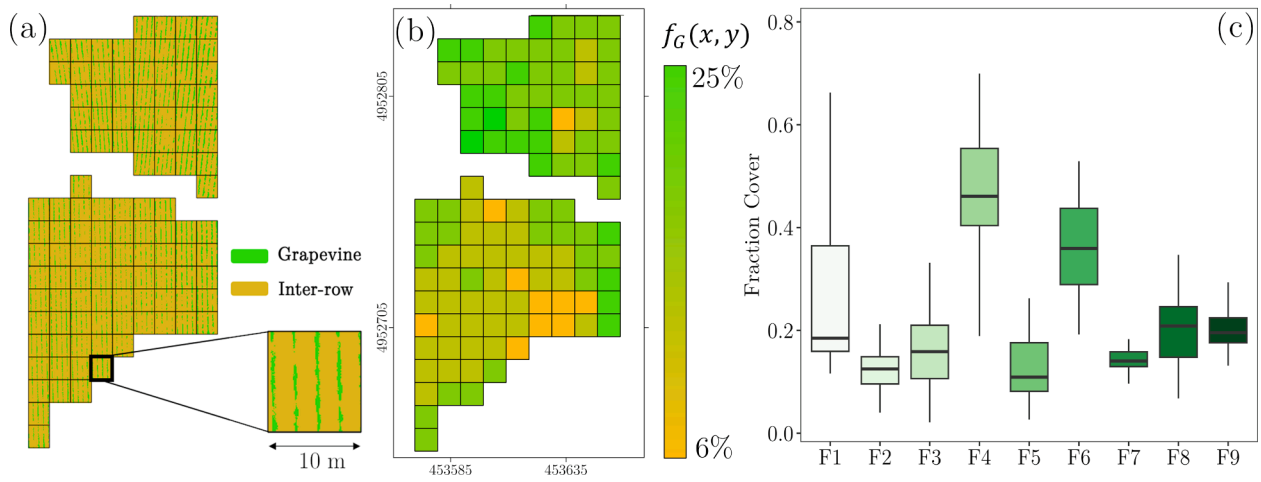

Fig. 3. (a) G-IR binary classification (GSD = 0.05 m) and the *G* graticule (vineyard F3); (b) $f_G(x,y)$ raster layer of F3 mapping the vines-related fraction cover; (c) boxplots (from bottom to the top lines are the 5th, 25th, 50th,75th, 95th percentiles) of $f_G(x,y)$ for all investigated vineyards. Reference coordinates system is WGS84/UTM 32 N.

computed using LMM (eq. (1). We can note that LMM NDVI values well fit the S2 ones ($R^2 = 0.87$). Moreover, applying this linear model resulting error is low (MAE = 0.03) and no significant bias is present. In fact, line offset is not significantly different from 0 ($t = 2.1$, $p > 0.05$). These results proved that linear mixture model using 2-endmembers assumption can be properly applied to NDVI values.

3.3. Recovering NDVI of vines through local least squares and reverse unmixing

Starting from the S2-derived NDVI map and $f_G(x,y)$, the local estimates of $\widehat{NDVI}_G$ and $\widehat{NDVI}_{IR}$ were computed applying the spatially–based local least squares approach of eq. (4) (Fig. 5a and 5b respectively). Eq. (5) was then used to map the theoretical uncertainty of estimates, i.e. $\sigma_G(x,y)$ and $\sigma_{IR}(x,y)$.

To provide an operative interpretation of these maps, F3 was selected as example. Considering Fig. 5a and 5b it can be noticed that NDVI estimates of vines are, generally, higher (mean value for all vineyards was 0.65) than the ones of inter-row zones (mean value for all vineyards was 0.25). This highly significant difference could be explained considering that local biomass and leaves system of vines are well developed in August, while inter-rows is continuously managed by mowing and, at

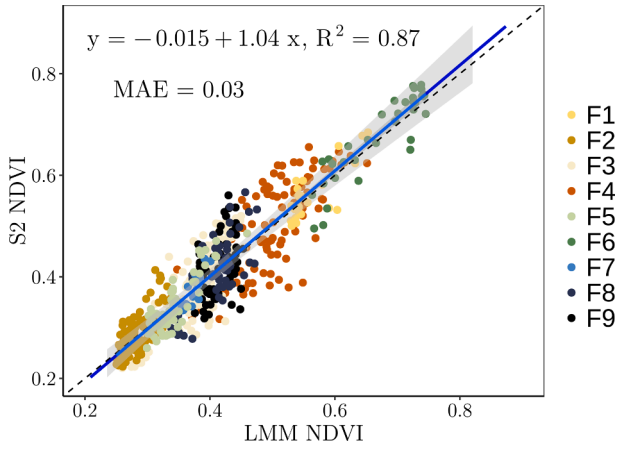

Fig. 4. Linear regression (blue line) between estimated NDVI values by LMM and correspondent S2 ones. Dotted line is 1:1 diagonal. Colored points are all pixels for each study vineyards. (For interpretation of the references to colour in this figure legend, the reader is referred to the web version of this article.)

that time of the year (especially in 2022), spontaneous vegetation is phenologically poorly active. Consider that in this part of Italy, vineyards are not irrigated. As far as maps of theoretical uncertainty are concerned (examples in Fig. 5c and 5d) these prove a direct proportionality between NDVI value and its uncertainty. In fact, the mean value of σ_G and σ_{IR} (in vineyard F3) were found to be 0.10 and 0.02, respectively.

Looking at all the investigated vineyards, $\widehat{NDVI}_G$ and $\widehat{NDVI}_{IR}$ statistical distributions were analyzed and the correspondent boxplot generated (Fig. 6a and 6b, respectively).

According to Fig. 6a, in general, one can note that the proposed unmixing method is able to recover well separated values of $\widehat{NDVI}_G$ and $\widehat{NDVI}_{IR}$. Vines NDVI values are always > 0.3, suggesting that a medium–high vegetation activity is present (Burgan, 1993; Ormsby et al., 1987; Zhang et al., 2003). Looking at Fig. 6b, it can be noticed that, in general, the median values of σ_G are always lower than 0.2 and that σ_{IR} are lower than σ_G. Specifically, the mean σ_G and σ_{IR} values were found to be 0.15 and 0.03, respectively. KS test proved that $\widehat{NDVI}_G$ and $\widehat{NDVI}_{IR}$ distributions were significantly different (Table 2) for all vineyards except for F6 where the separability is lower but significant.

Finally, to assess the spatial variability of estimates the coefficient of variation (CV%) was locally computed for each position of the moving window and the related mean and standard deviation values computed at vineyard level (see Fig. 7).

It can be noticed that a lower spatial variability (more homogeneous) is present concerning inter-row local estimates (CV% mean values always lower than 15 %). Specifically, the average CV% value in G and IR for all analyzed vineyards result to be 10 % and 18 % respectively. Furthermore, it should be highlighted that the highest grapevine CV% values are found in F5, F7 and F9 vineyards, with an average CV% value of 31 %, 33 % and 29 % respectively. This result suggests a low homogeneity within vines. Differently, inter-row CV% values appeared to be significantly lower compared to the row ones.

3.4. Validation

To test the reliability of estimates a comparison between $\widehat{NDVI}_G(x,y)$ and $\mu_G(x,y)$, was performed at vineyard level. MAPE values (Fig. 8) proved to be always lower than 16 % with a mean value of 10 %. Specifically, the vineyard showing the lowest and highest MAPE values were F4 (about 4 %) and F5 (about 16 %), respectively.

Testing the correlation about estimates and reference data, a significant one was found for all vineyards (Fig. 9): the majority of pixels, in

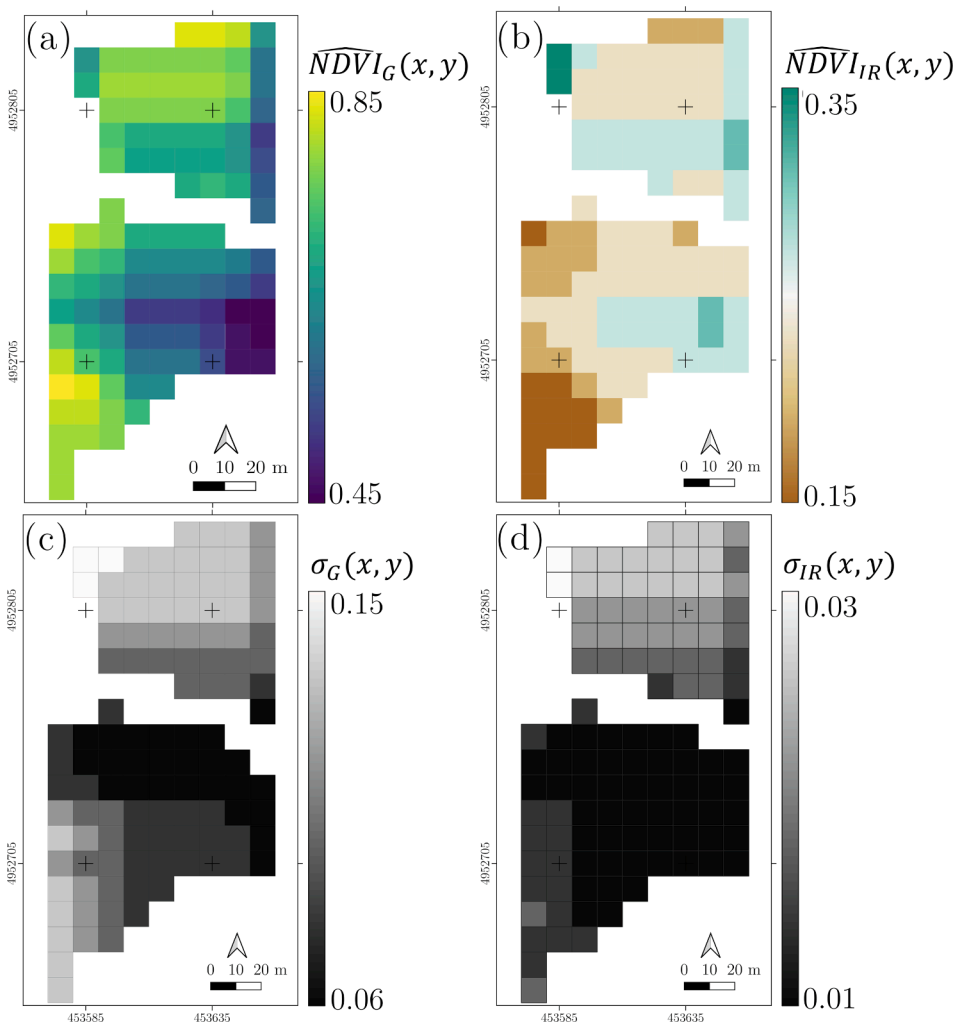

Fig. 5. (a-b) $\widehat{NDVI}_G(x,y)$ and $\widehat{NDVI}_{IR}(x,y)$ estimates (eq. (4)); (c-d) maps of the theoretical uncertainty of NDVI estimates, i.e. $\sigma_G(x,y)$ and $\sigma_{IR}(x,y)$, obtained by eq. (5). Reported maps refer to the F3 vineyard. Reference coordinates system is WGS84/UTM 32 N.

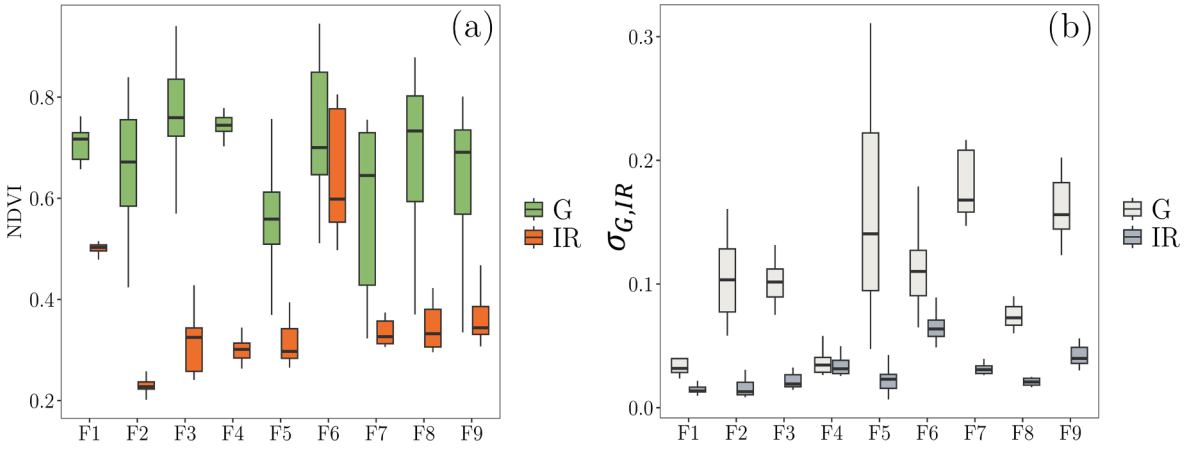

Fig. 6. (a) box-plots (5th, 25th, 50th,75th, 95th percentiles must be read bottom-up) of $\widehat{NDVI}_G(x,y)$ and $\widehat{NDVI}_{IR}(x,y)$ for all investigated vineyards; (b) box-plots of $\sigma_G(x,y)$ and $\sigma_{IR}(x,y)$ for all investigated vineyards.

fact, distribute closed to the bisecting line. Nevertheless, some values fail. Specifically, $\widehat{NDVI}_G$ values from vineyards F1, F3 and F4 appear to be the most consistent with reference data: the correspondent normalized density was in fact very high (>0.9). Differently, normalized density of vineyards F6, F7 and F8 was found to be very dispersed, making the correspondent $\widehat{NDVI}_G$ estimates less reliable.

This could be due to low variability of reference data, always around 0.70 and 0.80 NDVI values. Surprisingly, correspondent estimates cap-

Table 2
Separability between $\widehat{NDVI}_G$ and $\widehat{NDVI}_{IR}$ according to KS test.

Vineyard ID	D^+	p-value
F1	1.00	< 0.001
F2	1.00	< 0.001
F3	0.99	< 0.001
F4	1.00	< 0.001
F5	0.87	< 0.001
F6	0.40	< 0.01
F7	0.88	< 0.001
F8	0.89	< 0.001
F9	0.81	< 0.001

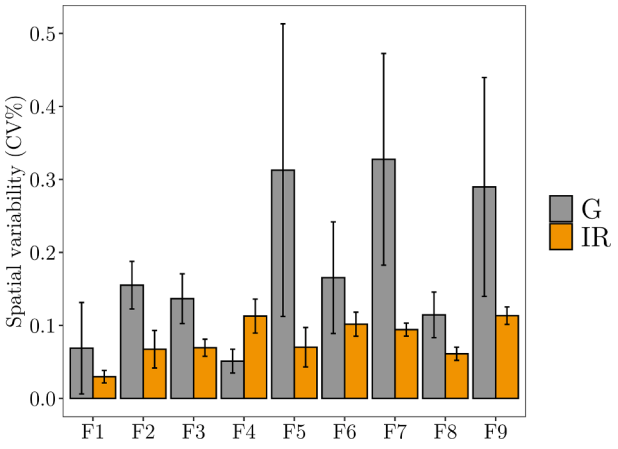

Fig. 7. Mean and mean ± 1 standard deviation of the local (CV%) computed at each position of the moving window, separately for G (grey bars) and IR (yellow bars) in the investigated vineyards. Bars are the mean values for each filed and whiskers are 1 standard deviation. (For interpretation of the references to colour in this figure legend, the reader is referred to the web version of this article.)

ture greater variability (elongated clouds in Fig. 9). This could be partially caused by a remaining contribution of inter-row in $\widehat{NDVI}_G$. Nevertheless, another explanation of this effects can be related to the reference layer, i.e. $\mu_G(x,y)$, itself. It is worth to remind that $\mu_G(x,y)$ is generated by mean operator involving $NDVI_G^{UAV}(x,y)$. This averaging procedure reduces the local NDVI variability of reference layer making more elongated/ biased the clouds in Fig. 9 if compared to proposed estimates.

Trying to qualify the nature of such errors, the bias-variance decomposition was applied at vineyard level considering all the pixels jointly. Fig. 10 shows the distributions of weights of $Bias^2$ and Tr.

Fig. 10 show that Tr has in general a higher weight than $Bias^2$, with median values always > 0.5). This suggests that the main error of $\widehat{NDVI}_G$ is related to σ_G.

It is worth to highlight that weight values are highly variable for both $Bias^2$ and Tr terms in vineyards F1, F4, F5 and F8. Differently, F6 showed a very small variability and the remaining ones the variability of the weights is limited.

3.5. Sensitivity analysis

Sensitivity analysis was performed to better explore the reliability of the proposed method. Since the method require that some hyper-parameters have to be set (i.e., the size of W and the Tikhonov regularization coefficient, λ). W size and λ value were iteratively changed and the correspondent solution and MAPE computed. This made possible to generate, at vineyard level, a 3D surface relating W, λ and MAPE. The optimal (W, λ values were set to the ones corresponding at the minimum value of MAPE. Fig. 11 shows the MAPE surface for the vineyard F3. It can be noted that the lowest MAPE value (11 %) is found for W and λ values equal to 9 and 0.01, respectively. Moreover, we can note that, in general, λ is very low denoting how regularization has a lower load on least square normal matrix diagonal. Concerning window size an average W parameter of 9 (±4) was found. If W is compared to field area it is interesting that on average, it is 11 % (±4%).

In Table 3 are summarized the W and λ values minimizing MAPE in all the investigated vineyards.

Concerning the assessment about the sensitivity of the proposed method to the precision of input parameters, i.e., $f_G(x,y)$ – one can also include the above-mentioned effects from – the K_2 parameter was considered and mapped across the vineyards. In Fig. 12 the K_2 map of F3 is reported (Fig. 12a) as an example, together with the statistical distributions of K_2 for all vineyards (Fig. 12b).

Considering Fig. 12b, it can be noted that a great variability within and among vineyards can be observed. The differences between the fields are significant, specifically in fields F2, F5, F7 and F9 K_2 values are around 20–25 %. On the contrary, in the other fields, K_2 values are around 7–10 %. Concerning K_2 value distribution within the fields, it turns out to be very variable in fields F2, F5 and F6. Conversely, it results to be almost 0 in field F4. Moreover, assuming an average K_2 value of 14 for all fields and applying the eq. (7), we can note how to maintain the theoretical relative error under 30 % we need a $f_G(x,y)$ layer having a relative precision of 3 %.

4. Discussions

4.1. Row / inter-row mapping and spectral linear mixture model

In this work the row area within an S2 pixel (GSD = 10 m) is about 20 %. Such a value may, however, differ across the area depending on the grape variety cultivated and the farmer's agronomic choices. The main differences, especially in the Italian wine context, are related to grape destination, planting pattern and consequently to cultivation site. For example, the Piemonte vineyard context is characterized by a large production of wine grapes (Asero and Patti, 2009). Specifically, to achieve excellent organoleptic qualities during vinification, the grape berries must be properly exposed to the sun. For this reason, in this area the vineyards are always cultivated in a vertical shoot position trellis system to maximize grape exposure. Conversely, in the southern part of Italy, which is characterized by having huge table grape cultivation, the high solar radiation (characterizing South-Italy), represents a problem for the grapes. Specifically, the main issue is grape-burning risk. To face this problem, farmers usually cultivate grapes in a free-standing grapevine (i.e. pergola) or adopts shade covers to mitigate the effect of the sun. With these premises, it is worth highlighting that row size ratio within a 10 m pixel can differ considerably. Actually, it is well known in literature that in vineyard having a vertical shoot position trellis system the presence of grapevine, and therefore of the row, is around 15–25 % (Gutiérrez-Gamboa et al., 2021; Hall et al., 2002). Delenne reports in his work that the distance between rows in a vineyard results to be around 2.5 m and the row canopy is around 0.5 m (Delenne et al., 2010). Consequently, in a pure vineyard S2 pixel there would be 2 m of row compared to the pixel's 10 m and consequently a row impact of 20 % as found in this work. On the other hand, in free-standing grapevines (e.g. pergola), the 'row' component can reach up to 100 % of S2 pixel coverage (Reynolds et al., 1996). In this case, however, all information derived from the vineyard through remote sensing could be attributed to the vineyard without using the spectra unmixing technique. Despite the differences in spatial resolution between open satellite missions like S2 and high-resolution UAV imagery, Nonni (Frederica et al., 2018) examined the relationship between these two instruments in the context of vertically trained vineyards. Their findings indicate that UAV imagery, once downsampled to 10 m resolution, highlight a strong correlation with the satellite imagery. Stolarski et al. (2022) and Matese et al. (2017) found similar results, although the pure canopy spectral

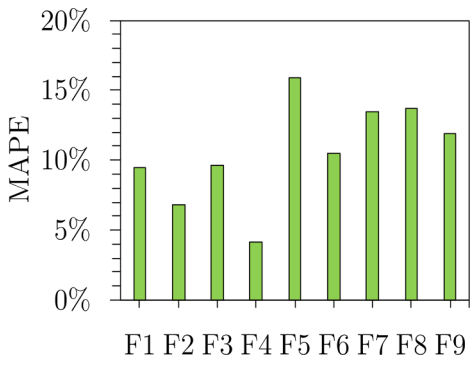

Fig. 8. MAPE of $\widehat{NDVI}_G(x,y)$ for investigated vineyards.

information did not correlate well with the S2 data. Furthermore, Matese et al. (2017) discovered that only the pure vine-related spectral information could effectively describe the water status, while the mixed spectral information could not. This highlights the need for a methodology to extract pure spectral information from satellite data for vertically trained vineyards. Conversely, Di Gennaro et al. (2019) used both S2 and UAV data to monitor productive parameters over overhead trained vineyards (Tendone), which show a vegetational cover close to 100 %. In this context, both UAV and S2 data achieved satisfactory results, demonstrating that the pixel-mixture monitoring problem only arises in vertically trained vineyards.

Otherwise, very little was found in the literature on spectral mixture in vineyards (Campos et al., 2014; Elmore et al., 2000; Hall et al., 2002). From these works, LMM is the most adopted. Unfortunately, in real scenarios, the electromagnetic radiation will interact with several components, leading to non-linear mixing between various components as a result of multiple scattering interactions (Heylen et al., 2014; Quintano et al., 2012). This could make LMM a biased approach. Furtherly, in this work we assumed only two endmembers, i.e., grapevine and inter-row. Therefore, to test LMM and two-endmembers assumptions within proposed approach, linear regression was fitted between S2 and UAV-derived NDVI values applying eq.1 (in Fig. 4). Results proved a very high correlation (Pearson's $r = 0.93$) and a good fitting ($R^2 = 0.87$). Moreover, applying a linear model to NDVI values a low error was found (MAE = 0.03). This finding is consistent with that of Campos et al. (2014) who applied LMM to NDVI values over vineyards and found a MAE of 0.03 between NDVI values retrieved from Landsat-5 and modeled ones. Moreover, two-endmembers assumption was also explored by Homayouni (Homayouni et al., 2008) where row-crops spectral unmixing for vigor monitoring was analyzed. These results support the hypothesis that LMM with 2-endmenmbers can be properly adopted to model spectral mixture in viticulture.

4.2. Recovering NDVI of vines through local least squares and reverse unmixing

In this framework, the present study was designed to isolate the only grapevine NDVI from the S2 one by a reverse unmixing procedure. The latter was here exploit by a local least squares approach involving k neighboring pixel within a moving window. As reported in Fig. 6 and tested by KS, $\widehat{NDVI}_G$ and $\widehat{NDVI}_{IR}$ are significant different and high separability is proved. It is worth to stress that $\widehat{NDVI}_G$ and $\widehat{NDVI}_{IR}$ are local estimates involving neighbor pixels. Therefore, they are local spatial average NDVI values at a given position. Nevertheless, this spatial variability was proved to be in general lower than 20 % and therefore can be assumed somehow representative of grapevine vigor (and phenology-related status) within a given S2 pixel. Despite this low average CV% values some differences within the row can be highlighted. This variability is exactly the one this approach is aiming at isolating and mapping in the phenological status monitoring framework. In fact, it is theoretically unthinkable to assume homogeneous conditions within and between fields. Crops are systematically affected by climatic, agronomic and terrain morphological conditions. Specifically, the latter is the one that maximizes the differences within the field. For example, terrain slope can play a positive or negative role in relation to irrigation in a vineyard. In AOI, plants located at the bottom of the area have more water resources. At the same time, the plants located to the higher areas have faster water drainage and the soil is subject to erosion (Tropeano, 1984). As water moves through the field, available nutrients also tend to settle in more or less specific areas. Furthermore, the structure and texture of the field can differ even in small fields. A field with a sandy area will allow greater water drainage, on the contrary, an area with a more clayey texture may cause water stagnation. Given all these differences, the farmer tries to homogenize the growing conditions of the vineyard through agronomic practices. Consequently, specific soil treatments, fertilizations and irrigations will be adopted to compensate for any deficits. Besides differences within the row, it was possible to note that inter-row CV% values were always lower than the row ones (Fig. 7).This is probably due to grapevine canopies that usually show a higher heterogeneity vigor than inter-row one (Campos et al., 2014; Khaliq et al., 2019; Sozzi et al., 2020). Moreover, inter-row management (e.g., mowing) is a factor to be taken into consideration. With this practice, it is possible to maintain constant and homogeneous within filed inter-row biomass (grass). This managed biomass generates additional benefits for grapevines as a higher vegetative growth, better canopy structure and nutrient content in petioles (Tesic et al., 2007). Therefore, inter-row biomass variability results lower than grapevine one. Consequently, it is much more difficult to highlight significant differences within this area.

4.3. Validation and sensitivity analysis

Validation of the proposed method performed by comparison to UAV-retrieved pure grapevine NDVI map shows high correlation (Fig. 9) and low MAPE values (<16 %) highlighting the effectiveness of the proposed approach. Nevertheless, fields from F5 to F9 show higher MAPE values than F1 to F4. These higher error rates are probably related to the heterogeneity of $\mu_G(x,y)$ values. In fact, we can note from Fig. 9 that same reference NDVI value, i.e., $\mu_G(x,y)$, correspond different $\widehat{NDVI}_G$. This can be caused by a lower separability between $\widehat{NDVI}_G$ and $\widehat{NDVI}_{IR}$ of fields F5 to F9 than F1 to F3 as supported by Fig. 6a and Table 2 that highlight poor separability for the formers.

A deeper error analysis shows that the majority of the error is caused by $\sigma_G(\varepsilon_{G,IR}(x,y)$ weights > 50 %, Fig. 10). F1 and F4 show lower biases while comparing estimates to reference NDVI values (Fig. 6a). This is also supported by Fig. 10 where the bias component is lower, reaching values lower than 0.3.

Sensitivity analysis has highlighted how the proposed method is affected by hyperparameters involved i.e., W and λ. Unfortunately, these

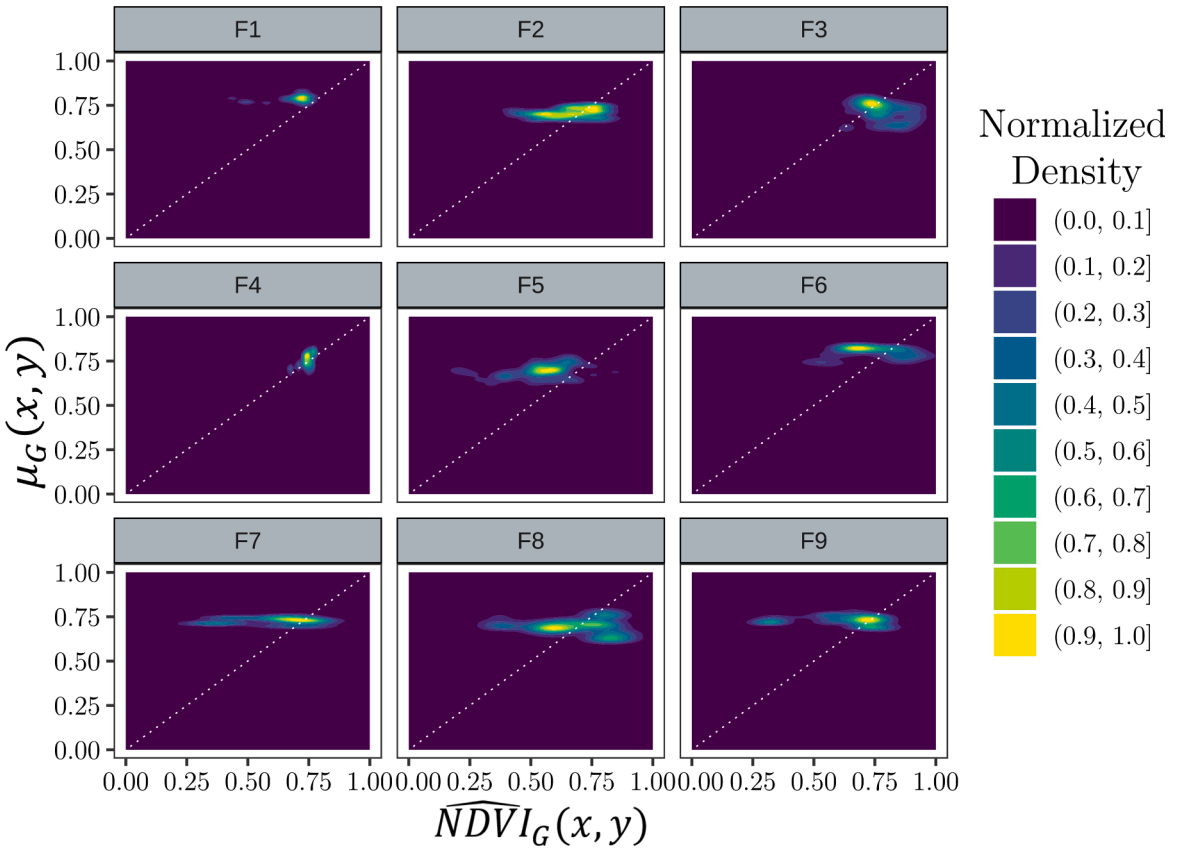

Fig. 9. Comparison between $\widehat{NDVI}_G$ and μ_G at vineyard level. Dotted line is the bisecting one. Colors bar shows the min–max normalized pixels density.

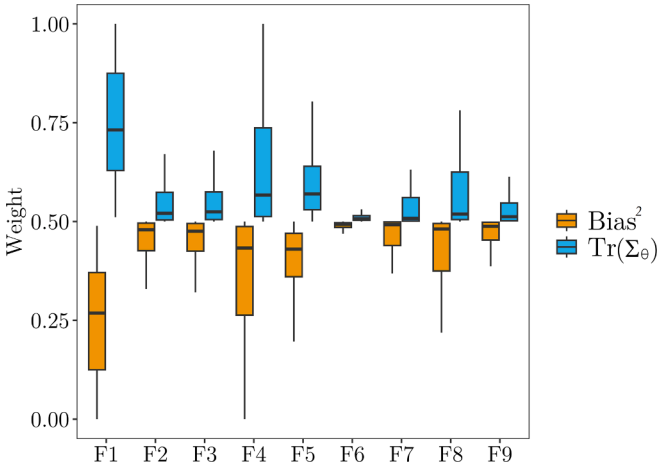

Fig. 10. Bias-variance decomposition of $[\varepsilon_{G,IR}(x,y)]^2$. Box-plots (5th, 25th, 50th,75th, 95th percentiles are given bottom-up) of weights concerning *Bias*^{2} and *Tr*.

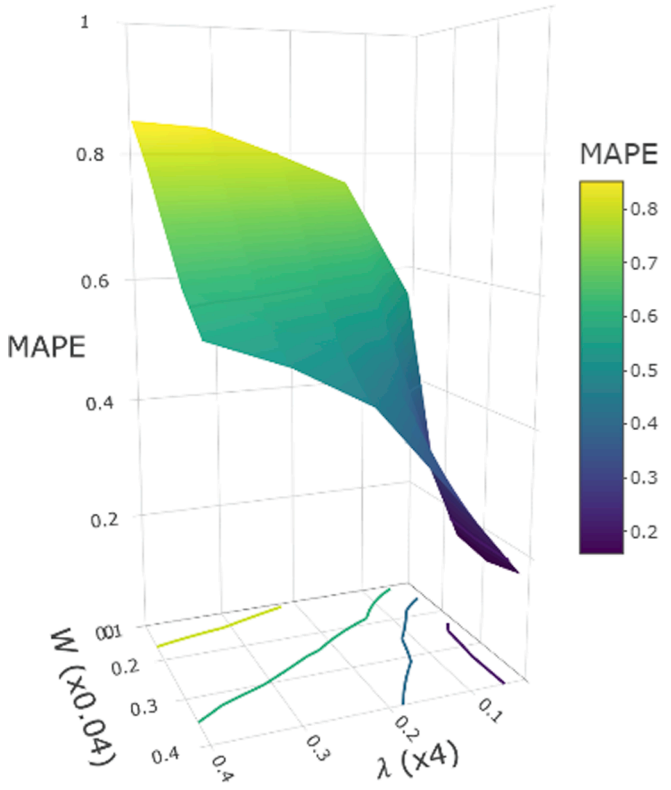

Fig. 11. MAPE *(W, λ)* surface as computed for the vineyard F3. Both *W* and *λ* values are scaled (reported values have to be dived by 0.04 and 4 for *W* and *λ* respectively).

are not *a-priori* known and they have to be properly tuned according to the faced application (Qian, 2017). Fortunately, both *W* and *λ* are not correlated to MAPE (Pearson's *r* is lower than 0.3) supporting a not-direct relationship of hyperparameters to errors. Otherwise, a negative relationship was found between K_2 and *λ* (Pearson's $r = -0.68$, p-value < 0.05). Increasing *λ*, K_2 values decrease. This is probably caused by Tikhonov regularization that adds loads to the least square normal matrix diagonal improving the system conditioning (Tikhonov, 1963). Unfortunately, higher *λ* values increase also $\varepsilon_{G,IR}(x,y)$ bias compromising estimates reliability. To overcome this problem, in this work, we

Table 3
W and λ values corresponding to the minimum value of MAPE for all the vineyards.

ID	W	% of vineyard area contained in W	λ
F1	7	18	0.01
F2	11	7	0.01
F3	9	7	0.10
F4	11	8	0.10
F5	9	7	0.01
F6	5	8	0.07
F7	5	14	0.01
F8	15	15	0.10
F9	15	14	0.01

properly tuned λ by *a-posteriori* validation. Results show that optimum λ values range between 0.01 and 0.1 making a $\varepsilon_{G,IR}(x,y)$ bias weight averagely equal to 35 %. Concerning W, it varies between 7 and 15 neighboring pixels. Despite this variability, comparing W in respect to field area, an W average value of 11 % was found in AOI.

Moreover, perturbation analysis based on condition index, reveals how the proposed method is affected by the precision of the input $f_G(x,y)$ layer. In fact, K_2 maps (Fig. 12a) provides information about the stability of numerical solutions for each moving window step. In particular, it relates the percentage error of $f_G(x,y)$ to the percentage error of the output (i.e., $\widehat{NDVI}_G$). We can note that in AOI an average K_2 values of 14 was found. Assuming a tolerable relative error of NDVI estimate lower than 30 %, a very precise fraction cover values mapping grapevine canopies with a precision of about 3 % is mandatory. This high precision highlights the need for a high-resolution 3D survey of vineyard useful to proficient apply the proposed approach. This constitutes the main limitation of proposed method requiring that $f_G(x,y)$ is mapped with high geometric accuracy, otherwise the unmixing procedure leads to unreliable estimates as proved by sensitivity analysis. Nevertheless, in this work, $f_G(x,y)$ was computed starting from an UAV photogrammetric acquisition. The latter is a common adopted techniques in viticulture as proved by a review performed by Singh (Singh et al., 2022). Furthermore, currently RGB sensors plugged on an airborne platform guarantee a cost-effective 3D survey (Borgogno Mondino and Gajetti, 2017; De Petris et al., 2020) providing images with very high precision as highlighted by several authors (Matese and Di Gennaro, 2021; Sarvia et al., 2021; Singh et al., 2022). The adoption of S2 data allows to freely collect NDVI maps with a global coverage and early update (Shukla et al., 2019) (S2 temporal resolution is 5 days). Therefore, the approach here proposed can be reproduced once $f_G(x,y)$ maps derived by UAV high resolution survey is performed. Future improvements will explore how $f_G(x,y)$ temporal variability during a phenological season can affect the reverse spectral unmixing procedure based on least squares.

It is interesting to note how literature about remote sensing images-based spectral unmixing on row-crops is very limited. Borgogno-Mondino (2022) applied a spectra unmixing procedure on pomegranate orchards to separate row NDVI values from the inter-rows ones using Sentinel-2 data. Unfortunately, this method relies on the adoption of pure rows endmember spectrum that ordinarily is difficult to retrieve without a ground based spectroradiometric survey. Somers et al. (2009) analyzed orchards adopting a non-linear hyperspectral mixture analysis to separate tree cover from the mixed signal. Nevertheless, only tree cover estimates were derived without focusing on tree spectra mapping. Conversely, our proposed approach tries to fill the above-mentioned gaps mapping NDVI of vines only signal, also providing uncertainty values of estimates. Given this literature gap, this study would like to point out the importance of taking care about spectra mixture while working with satellite remote sensing on row-crops like vineyards or orchards, stimulating further research on this issue.

5. Conclusions

Vineyard row and inter-row mapping is crucial step while working with satellite remotely sensed images in viticulture and deriving information are useful to support the agronomic practices. Nevertheless, vineyards represent a challenge in this context because grapevine canopies are discontinuous and therefore, spectral mixture between grapevine canopies, and inter-row is expected within a satellite-derived pixel. Not considering this issue can drive to wrong deductions and misguided treatments. In this work, a possible solution was proposed based on local least squares and reverse unmixing procedure. Once mapped rows and interrow proportions within S2 pixel, starting from $NDVI^{S2}$ local $\widehat{NDVI}_G$ and $\widehat{NDVI}_{IR}$ can be properly mapped. Resulted maps have a MAPE always lower than 16 % highlighting the effectiveness of proposed approach. Unfortunately, sensitivity analysis showed strong dependency from W and λ hypermeters. Moreover, accurate fraction cover estimates (i.e., $f_G(x,y)$) are need. These can currently be mapped only by high resolution UAV survey. Nevertheless, this type of survey is increasingly adopted in viticulture and proficiently combined with S2 data makes it possible to applied proposed approach in different

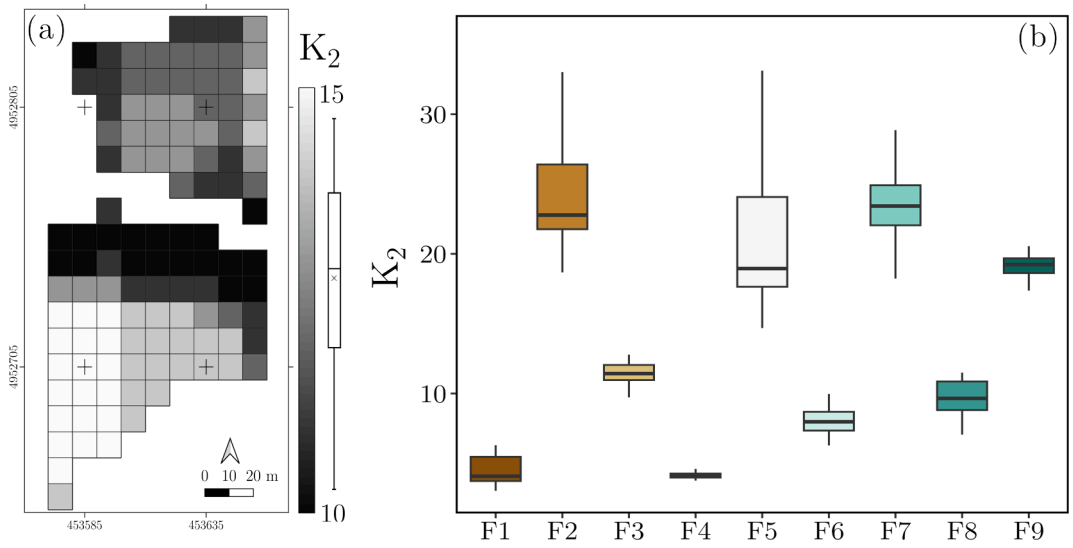

Fig. 12. (a) K_2 map of F3 and related box-plot of K_2 values distribution (cross is the mean). Reference coordinates system is WGS84/UTM 32 N. (b) Box-plots (5th, 25th, 50th,75th, 95th percentiles must be read bottom-up) of K_2 values for all vineyards.

agronomic contexts allowing a phenological monitoring of grapevine combining the high temporal resolution provided by earth observation imagery.

Funding

This research was supported by the European Agricultural Fund for Rural Development and within Piemonte Region PSR 2014–2020. Project title: “Integrated Tools for the Environmental Sustainability of the Vineyard (SISAV)”. Grant number: 20201144522.

CRediT authorship contribution statement

S. De Petris: Writing – review & editing, Writing – original draft, Validation, Software, Methodology, Investigation, Formal analysis, Data curation, Conceptualization. **F. Sarvia:** Writing – original draft, Validation, Formal analysis, Data curation. **F. Parizia :** Writing – original draft, Validation, Software, Formal analysis, Data curation. **F. Ghilardi:** Writing – original draft, Validation, Formal analysis, Data curation. **A. Farbo:** Writing – original draft, Validation, Formal analysis, Data curation. **E. Borgogno-Mondino:** Writing – review & editing, Supervision, Resources, Project administration, Methodology, Conceptualization.

Declaration of competing interest

The authors declare the following financial interests/personal relationships which may be considered as potential competing interests: Enrico Borgogno-Mondino reports financial support was provided by European Agricultural Fund for Rural Development. If there are other authors, they declare that they have no known competing financial interests or personal relationships that could have appeared to influence the work reported in this paper.

Data availability

Data will be made available on request.

Acknowledgements

We would like to thank Dr. Virano Andrea for his precious support in UAV surveys.

Appendix A. Supplementary material

Supplementary data to this article can be found online at https://doi.org/10.1016/j.compag.2024.109092.

References

Anagrafe agricola del Piemonte - Sistema Piemonte - Regione Piemonte. Available online: https://servizi.regione.piemonte.it/catalogo/anagrafe-agricola-piemonte (Accessed on 25/05/2023), n.d.

Asero, V., Patti, S., 2009. From wine production to wine tourism experience: the case of Italy.

Assumma, V., Bottero, M., Monaco, R., 2016. Landscape economic value for territorial scenarios of change: an application for the Unesco site of Langhe, Roero and Monferrato. Proc.-Soc. Behav. Sci. 223, 549–554.

Baboulin, M., Dongarra, J., Gratton, S., Langou, J., 2009. Computing the conditioning of the components of a linear least-squares solution. Numer. Linear Algebra Appl. 16, 517–533.

Bagagiolo, G., Biddoccu, M., Rabino, D., Cavallo, E., 2018. Effects of rows arrangement, soil management, and rainfall characteristics on water and soil losses in Italian sloping vineyards. Environ. Res. 166, 690–704.

Biddoccu, M., Ferraris, S., Cavallo, E., Opsi, F., Previati, M., Canone, D., 2013. Hillslope vineyard rainfall-runoff measurements in relation to soil infiltration and water content. Proc. Environ. Sci. 19, 351–360.

Biddoccu, M., Opsi, F., Cavallo, E., 2014. Relationship between runoff and soil losses with rainfall characteristics and long-term soil management practices in a hilly vineyard (Piedmont, NW Italy). Soil Sci. Plant Nutr. 60, 92–99.

Borgogno Mondino, E., 2018. Remote sensing from RPAS in agriculture: an overview of expectations and unanswered questions. Mech. Mach. Sci. 49, 483–492. https://doi.org/10.1007/978-3-319-61276-8_51.

Borgogno Mondino, E., Gajetti, M., 2017. Preliminary considerations about costs and potential market of remote sensing from UAV in the Italian viticulture context. Eur. J. Remote Sens. 50, 310–319. https://doi.org/10.1080/22797254.2017.1328269.

Borgogno-Mondino, E., Farbo, A., Novello, V., de Palma, L., 2022. A fast regression-based approach to map water status of pomegranate orchards with sentinel 2 data. Horticulturae 8, 759. https://doi.org/10.3390/horticulturae8090759.

Borgogno-Mondino, E., Fissore, V., 2022. Reading greenness in urban areas: possible roles of phenological metrics from the Copernicus HR-VPP dataset. Remote Sens. (Basel) 14, 4517. https://doi.org/10.3390/rs14184517.

Borgogno-Mondino, E., Sarvia, F., Gomarasca, M.A., 2019. Supporting insurance strategies in agriculture by remote sensing: a possible approach at regional level. In: International Conference on Computational Science and Its Applications. Springer, pp. 186–199.

Bouckaert, R.R., 2008. Practical bias variance decomposition. In: AI 2008: Advances in Artificial Intelligence: 21st Australasian Joint Conference on Artificial Intelligence Auckland, New Zealand, December 1-5, 2008. Proceedings 21. Springer, pp. 247–257.

Burgan, R.E., 1993. Monitoring Vegetation Greenness with Satellite Data. US Department of Agriculture, Forest Service, Intermountain Research Station.

Campos, I., Neale, C.M., López, M.-L., Balbontín, C., Calera, A., 2014. Analyzing the effect of shadow on the relationship between ground cover and vegetation indices by using spectral mixture and radiative transfer models. J. Appl. Remote Sens. 8, 083562.

Clasen, A., Somers, B., Pipkins, K., Tits, L., Segl, K., Brell, M., Kleinschmit, B., Spengler, D., Lausch, A., Förster, M., 2015. Spectral unmixing of forest crown components at close range, airborne and simulated Sentinel-2 and EnMAP spectral imaging scale. Remote Sens. (Basel) 7, 15361–15387.

De Petris, S., Sarvia, F., Borgogno-Mondino, E., 2020. RPAS-based photogrammetry to support tree stability assessment: Longing for precision arboriculture. Urban For. Urban Green. 55, 126862.

De Petris, S., Squillacioti, G., Bono, R., Borgogno-Mondino, E., 2021. Geomatics and epidemiology: associating oxidative stress and greenness in urban areas. Environ. Res. 197, 110999 https://doi.org/10.1016/j.envres.2021.110999.

Delenne, C., Durrieu, S., Rabatel, G., Deshayes, M., 2010. From pixel to vine parcel: a complete methodology for vineyard delineation and characterization using remote-sensing data. Comput. Electron. Agric. 70, 78–83.

Di Gennaro, S.F., Dainelli, R., Palliotti, A., Toscano, P., Matese, A., 2019. Sentinel-2 validation for spatial variability assessment in overhead trellis system viticulture versus UAV and agronomic data. Remote Sens. (Basel) 11, 2573.

DJI, 2023. DJI - P4 Multispectral [WWW Document]. URL https://www.dji.com/it/p4-multispectral.

Domingos, P., 2000. A unified bias-variance decomposition. In: Proceedings of 17th International Conference on Machine Learning. Morgan Kaufmann Stanford, pp. 231–238.

Elmore, A.J., Mustard, J.F., Manning, S.J., Lobell, D.B., 2000. Quantifying vegetation change in semiarid environments: precision and accuracy of spectral mixture analysis and the normalized difference vegetation index. Remote Sens. Environ. 73, 87–102.

Farbo, A., Sarvia, F., De Petris, S., Borgogno-Mondino, E., 2022. Preliminary Concerns about Agronomic Interpretation of NDVI Time Series From Sentinel-2 Data: Phenology and Thermal Efficiency of Winter Wheat in Piemonte (NW Italy). Int. Arch. Photogramm. Remote. Sens. Spat. Inf. Sci. 43, 863–870.

Ferreiro-Arman, M., Da Costa, J.-P., Homayouni, S., Martin-Herrero, J., 2006. Hyperspectral image analysis for precision viticulture. In: International Conference Image Analysis and Recognition. Springer, pp. 730–741.

Filippo, S., Samuele, D.P., Enrico, B.-M., 2022. Detection and counting of meadow cuts by copernicus sentinel-2 imagery in the framework of the common agricultural policy (CAP). Eur. J. Remote Sens. 1–15.

Forlani, G., Dall’Asta, E., Diotri, F., di Cella, U.M., Roncella, R., Santise, M., 2018. Quality Assessment of DSMs Produced from UAV Flights Georeferenced with On-Board RTK Positioning. Remote Sens. (Basel) 10. https://doi.org/10.3390/rs10020311.

Frederica, N., Malacarne, D.F., Pappalardo, S., Codato, D., Meggio, F., De Marchi, M., 2018. Sentinel-2 data analysis and comparison with UAV multispectral images for precision viticulture. GI FORUM. 105–116.

Giovos, R., Tassopoulos, D., Kalivas, D., Lougkos, N., Priovolou, A., 2021. Remote sensing vegetation indices in viticulture: a critical review. Agriculture 11, 457. https://doi.org/10.3390/agriculture11050457.

Greatrex, H., Hansen, J., Garvin, S., Diro, R., Blakeley, S., Guen, M.L., Rao, K., Osgood, D., n.d. Scaling up index insurance for smallholder farmers: 32.

Gutiérrez-Gamboa, G., Zheng, W., Martinez de Toda, F., 2021. Strategies in vineyard establishment to face global warming in viticulture: a mini review. J. Sci. Food Agric. 101, 1261–1269.

Hall, A., Lamb, D.W., Holzapfel, B., Louis, J., 2002. Optical remote sensing applications in viticulture-a review. Aust. J. Grape Wine Res. 8, 36–47.

Hall, A., Louis, J.P., Lamb, D.W., 2008. Low-resolution remotely sensed images of winegrape vineyards map spatial variability in planimetric canopy area instead of leaf area index. Aust. J. Grape Wine Res. 14, 9–17.

Helman, D., Bahat, I., Netzer, Y., Ben-Gal, A., Alchanatis, V., Peeters, A., Cohen, Y., 2018. Using Time Series of High-Resolution Planet Satellite Images to Monitor Grapevine Stem Water Potential in Commercial Vineyards. Remote Sens. (Basel) 10, 1615. https://doi.org/10.3390/rs10101615.

Heylen, R., Parente, M., Gader, P., 2014. A review of nonlinear hyperspectral unmixing methods. IEEE J. Sel. Top. Appl. Earth Obs. Remote Sens. 7, 1844–1868.
Hoerl, A.E., Kannard, R.W., Baldwin, K.F., 1975. Ridge regression: some simulations. Commun. Statistics-Theory Methods 4, 105–123.
Homayouni, S., Germain, C., Lavialle, O., Grenier, G., Goutouly, J.-P., Van Leeuwen, C., Da Costa, J.-P., 2008. Abundance weighting for improved vegetation mapping in row crops: application to vineyard vigour monitoring. Can. J. Remote. Sens. 34, S228–S239.
Hu, Y.H., Lee, H.B., Scarpace, F.L., 1999. Optimal linear spectral unmixing. IEEE Trans. Geosci. Remote Sens. 37, 639–644.
Jia, Z., Li, B., 2013. On the condition number of the total least squares problem. Numer. Math. 125, 61–87.
Johnson, L.F., Roczen, D.E., Youkhana, S.K., Nemani, R.R., Bosch, D.F., 2003. Mapping vineyard leaf area with multispectral satellite imagery. Comput. Electron. Agric. 38, 33–44.
Karakizi, C., Oikonomou, M., Karantzalos, K., 2016. Vineyard detection and vine variety discrimination from very high resolution satellite data. Remote Sens. (Basel) 8, 235.
Kaul, H.A., Sopan, I., 2012. Land use land cover classification and change detection using high resolution temporal satellite data. J. Environ. 1, 146–152.
Khaliq, A., Comba, L., Biglia, A., Ricauda Aimonino, D., Chiaberge, M., Gay, P., 2019. Comparison of satellite and UAV-based multispectral imagery for vineyard variability assessment. Remote Sens. (Basel) 11, 436.
Marshall, M., Belgiu, M., Boschetti, M., Pepe, M., Stein, A., Nelson, A., 2022. Field-level crop yield estimation with PRISMA and Sentinel-2. ISPRS J. Photogramm. Remote Sens. 187, 191–210.
Matese, A., Di Gennaro, S.F., 2021. Beyond the traditional NDVI index as a key factor to mainstream the use of UAV in precision viticulture. Sci. Rep. 11, 2721.
Matese, A., Di Gennaro, S.F., Miranda, C., Berton, A., Santesteban, L.G., 2017. Evaluation of spectral-based and canopy-based vegetation indices from UAV and Sentinel 2 images to assess spatial variability and ground vine parameters. Adv. Anim. Biosci. 8, 817–822.
Misra, G., Cawkwell, F., Wingler, A., 2020. Status of phenological research using Sentinel-2 data: A review. Remote Sens. (Basel) 12, 2760.
Narmilan, A., Gonzalez, F., Salgadoe, A.S.A., Powell, K., 2022. Detection of white leaf disease in sugarcane using machine learning techniques over UAV multispectral images. Drones 6. https://doi.org/10.3390/drones6090230.
Nesbit, P.R., Hubbard, S.M., Hugenholtz, C.H., 2022. Direct georeferencing UAV-SfM in high-relief topography: accuracy assessment and alternative ground control strategies along steep inaccessible rock slopes. Remote Sens. (Basel) 14. https://doi.org/10.3390/rs14030490.
Ormsby, J.P., Choudhury, B.J., Owe, M., 1987. Vegetation spatial variability and its effect on vegetation indices. Int. J. Remote Sens. 8, 1301–1306.
Pádua, L., Matese, A., Di Gennaro, S.F., Morais, R., Peres, E., Sousa, J.J., 2022. Vineyard classification using OBIA on UAV-based RGB and multispectral data: A case study in different wine regions. Comput. Electron. Agric. 196, 106905.
Pastick, N.J., Dahal, D., Wylie, B.K., Parajuli, S., Boyte, S.P., Wu, Z., 2020. Characterizing land surface phenology and exotic annual grasses in dryland ecosystems using landsat and sentinel-2 data in harmony. Remote Sens. (Basel) 12, 725.
Phiri, D., Simwanda, M., Salekin, S., Nyirenda, V.R., Murayama, Y., Ranagalage, M., 2020. Sentinel-2 data for land cover/use mapping: a review. Remote Sens. (Basel) 12, 2291. https://doi.org/10.3390/rs12142291.
PIX4D Support, 2023. Radiometric Processing and Calibration [WWW Document]. URL https://support.pix4d.com/hc/en-us/articles/203891879-Menu-Process-Processing-Options-3-DSM-Orthomosaic-and-Index-Index-Calculator#label3 (accessed 5.18.23).
Priori, S., Martini, E., Andrenelli, M.C., Magini, S., Agnelli, A.E., Bucelli, P., Biagi, M., Pellegrini, S., Costantini, E.A.C., 2013. Improving wine quality through harvest zoning and combined use of remote and soil proximal sensing. Soil Sci. Soc. Am. J. 77, 1338–1348.
Qian, K., 2017. On the determination of proper regularization parameter: α-weighted BLE via A-optimal design and its comparison with the results derived by numerical methods and ridge regression (B.S. thesis).
Quintano, C., Fernández-Manso, A., Shimabukuro, Y.E., Pereira, G., 2012. Spectral unmixing. Int. J. Remote Sens. 33, 5307–5340.
R Development Core Team, R., 2013. R: A language and environment for statistical computing.
Rahman, M.M., Robson, A., Bristow, M., 2018. Exploring the Potential of High Resolution WorldView-3 Imagery for Estimating Yield of Mango. Remote Sens. (Basel) 10, 1866. https://doi.org/10.3390/rs10121866.
Reynolds, A.G., Wardle, D.A., Naylor, A.P., 1996. Impact of training system, vine spacing, and basal leaf removal on Riesling. Vine performance, berry composition, canopy microclimate, and vineyard labor requirements. Am. J. Enol. Vitic. 47, 63–76.
Sakamoto, T., Ogawa, D., Hiura, S., Iwasaki, N., 2022. Alternative procedure to improve the positioning accuracy of orthomosaic images acquired with agisoft metashape and DJI P4 multispectral for crop growth observation. Photogramm. Eng. Remote Sens. 88, 323–332. https://doi.org/10.14358/PERS.21-00064R2.
Sarvia, F., De Petris, S., Borgogno-Mondino, E., 2020. Multi-scale remote sensing to support insurance policies in agriculture: from mid-term to instantaneous deductions. Null 57, 770–784. https://doi.org/10.1080/15481603.2020.1798600.
Sarvia, F., Petris, S.D., Orusa, T., Borgogno-Mondino, E., 2021. MAIA S2 Versus Sentinel 2: Spectral Issues and Their Effects in the Precision Farming Context. In: International Conference on Computational Science and Its Applications. Springer, pp. 63–77.
Sarvia, F., De Petris, S., Borgogno-Mondino, E., 2022a. Mapping ecological focus areas within the EU CAP controls framework by Copernicus Sentinel-2 data. Agronomy 12, 406.
Sarvia, F., De Petris, S., Ghilardi, F., Xausa, E., Cantamessa, G., Borgogno-Mondino, E., 2022b. The importance of agronomic knowledge for crop detection by Sentinel-2 in the CAP controls framework: a possible rule-based classification approach. Agronomy 12, 1228. https://doi.org/10.3390/agronomy12051228.
Segarra, J., Buchaillot, M.L., Araus, J.L., Kefauver, S.C., 2020. Remote sensing for precision agriculture: Sentinel-2 improved features and applications. Agronomy 10, 641.
Shukla, G., Garg, R.D., Garg, P.K., Srivastava, H.S., Kumar, P., Mohanty, B., 2019. Exploring the capabilities of sentinel-2 data in vegetation health/stress mapping. In: IGARSS 2019–2019 IEEE International Geoscience and Remote Sensing Symposium. IEEE, pp. 6652–6655.
Singh, A.P., Yerudkar, A., Mariani, V., Iannelli, L., Glielmo, L., 2022. A bibliometric review of the use of unmanned aerial vehicles in precision agriculture and precision viticulture for sensing applications. Remote Sens. (Basel) 14, 1604.
Somers, B., Cools, K., Delalieux, S., Stuckens, J., Van der Zande, D., Verstraeten, W.W., Coppin, P., 2009. Nonlinear hyperspectral mixture analysis for tree cover estimates in orchards. Remote Sens. Environ. 113, 1183–1193.
Soriano-González, J., Angelats, E., Martínez-Eixarch, M., Alcaraz, C., 2022. Monitoring rice crop and yield estimation with Sentinel-2 data. Field Crop Res 281, 108507.
Sozzi, M., Kayad, A., Marinello, F., Taylor, J., Tisseyre, B., 2020. Comparing vineyard imagery acquired from Sentinel-2 and Unmanned Aerial Vehicle (UAV) platform. Oeno One 54, 189–197.
Stolarski, O., Fraga, H., Sousa, J.J., Pádua, L., 2022. Synergistic use of Sentinel-2 and UAV multispectral data to improve and optimize viticulture management. Drones 6, 366.
Teppati Losè, L., Chiabrando, F., Giulio Tonolo, F., 2020. Boosting the timeliness of UAV large scale mapping. direct georeferencing approaches: operational strategies and best practices. ISPRS Int. J. Geo Inf. 9 https://doi.org/10.3390/ijgi9100578.
Tesic, D., Keller, M., Hutton, R.J., 2007. Influence of vineyard floor management practices on grapevine vegetative growth, yield, and fruit composition. Am. J. Enol. Vitic. 58, 1–11.
Tikhonov, A.N., 1963. On the solution of ill-posed problems and the method of regularization. In: Doklady Akademii Nauk. Russian Academy of Sciences, pp. 501–504.
Tropeano, D., 1984. Rate of soil erosion processes on vineyards in Central Piedmont (NW Italy). Earth Surf. Proc. Land. 9, 253–266.
Van Beek, J., Tits, L., Somers, B., Coppin, P., 2013. Stem water potential monitoring in pear orchards through WorldView-2 multispectral imagery. Remote Sens. (Basel) 5, 6647–6666. https://doi.org/10.3390/rs5126647.
Wang, N., Guo, Y., Wei, X., Zhou, M., Wang, H., Bai, Y., 2022. UAV-based remote sensing using visible and multispectral indices for the estimation of vegetation cover in an oasis of a desert. Ecol. Ind. 141, 109155 https://doi.org/10.1016/j.ecolind.2022.109155.
Westoby, M.J., Brasington, J., Glasser, N.F., Hambrey, M.J., Reynolds, J.M., 2012. 'Structure-from-Motion' photogrammetry: a low-cost, effective tool for geoscience applications. Geomorphology 179, 300–314. https://doi.org/10.1016/j.geomorph.2012.08.021.
Winkler, A.J., 1969. Effect of vine spacing in an unirrigated vineyard on vine physiology, production and wine quality. Am. J. Enol. Vitic. 20, 7–15.
Zhang, X., Friedl, M.A., Schaaf, C.B., Strahler, A.H., Hodges, J.C., Gao, F., Reed, B.C., Huete, A., 2003. Monitoring vegetation phenology using MODIS. Remote Sens. Environ. 84, 471–475.